WORLD–LINE QUANTUM MONTE CARLO

R.T. SCALETTAR
Physics Department
One Shields Ave.
University of California
Davis, CA 95616

Abstract. In this chapter we describe the "World–Line" Quantum Monte Carlo algorithm, primarily for quantum spin, boson, and fermion models on a lattice. We will take a rather broad definition of this approach to include any simulation in which a path–integral expression for the partition function is written down by discretizing the inverse temperature β, introducing complete sets of intermediate states, and then summing over those states stochastically. Because expositions of the world–line algorithm already exist in the literature for quantum spin and fermion systems, we will focus on recent applications of the method to interacting boson Hamiltonians.

1. Introduction

Finite temperature Quantum Monte Carlo methods employ path integrals to map the partition function for quantum mechanical systems onto equivalent classical models in one higher dimension. In the world–line method,[1] the resulting classical degrees of freedom are the eigenvalues of the original quantum operators. The world–line algorithm follows the evolution of these eigenvalues in imaginary time τ, for example the position $x_n(\tau)$ of oscillator n for a system of quantum oscillators, or the z component $S^z_n(\tau)$ of spin n for a set of quantum spins. One of the most attractive features of the approach is precisely that these world–lines trace variables which are associated with the operators in the original quantum Hamiltonian and therefore allow a very intuitive real space picture of the correlations in the system. In contrast, the determinant Monte Carlo algorithm, which is the focus of other chapters in this volume, also begins with a mapping of a quantum problem onto a classical problem in one higher dimension, but

the resulting classical degrees of freedom are less directly related to the original operators in the Hamiltonian.[2]

The organization of this chapter is as follows: We will first write down the world–line path integral representation of a single anharmonic quantum oscillator. This problem shares many features of more complicated models, for example the nature of errors associated with discretizing β and the possibility of long correlation times in simulations. However, exact analytic analysis is possible, making it a good way to develop an intuition concerning path integral simulations. Additionally, once the single oscillator action is determined, the action for related, physically interesting, interacting many body systems can be written down by inspection. We will next discuss the problem of the 1–d Ising model in a transverse magnetic field, whose associated classical model is the anisotropic 2d Ising model. From known analytic solutions of the classical model, we can immediately determine the phase diagram of the quantum system. This illustrates how the path integral formalism itself can reveal insights into the physics even before detailed numerical work is begun. Finally, we will turn to lattice quantum spin, boson, and fermion models where the classical action is still local, but considerably more complicated.

We will assume that the reader is already familiar with Monte Carlo for problems in classical statistical mechanics, and not describe that here. Nor will we discuss generalizations of the most elementary local "moves" by which world–line Monte Carlo explores phase space. Such "cluster" or "loop" algorithms are, however, in many cases much more efficient methods to evolve the degrees of freedom.[3]

2. The Quantum Oscillator

Consider a single anharmonic quantum oscillator.[4, 5] The partition function is,

$$\begin{aligned} Z &= \mathrm{Tr}\ e^{-\beta \hat{H}} \\ \hat{H} &= \frac{\hat{P}^2}{2m} + \frac{1}{2} m\omega^2 \hat{X}^2 + \frac{1}{4}\lambda \hat{X}^4. \end{aligned} \tag{1}$$

For $\lambda \neq 0$, we do not know how to evaluate the exponential of the entire Hamiltonian, but we do know how to evaluate the exponential of the kinetic and potential energies separately. Unfortunately, since $\hat{X}$ and $\hat{P}$ do not commute, we cannot break up the exponential of $\hat{H}$ into a product of exponentials. We therefore proceed as follows: We discretize the imaginary time β into L smaller subintervals of length $\Delta\tau$, that is, $\beta = L\Delta\tau$. We can then write,

$$Z_{\mathrm{tr}} = \mathrm{Tr}\ [e^{-\Delta\tau \hat{P}^2/2m} e^{-\Delta\tau m\omega^2 \hat{X}^2/2 - \Delta\tau\lambda\hat{X}^4/4}]^L \tag{2}$$

In the limit $\Delta\tau \to 0$ (or, equivalently, $L \to \infty$), we have $Z_{\rm tr} \to Z$. Using $Z_{\rm tr}$ in place of Z for finite $\Delta\tau$ is referred to as the "Suzuki-Trotter" approximation.[6, 7, 8] We have appended the subscript "tr" to Z to distinguish the approximate expression obtained at finite L from the exact one for $L = \infty$. We will discuss in detail the effect of finite $\Delta\tau$, but for the moment we only emphasize that this is a controlled approximation in the sense that by making $\Delta\tau$ increasingly small we can reduce the error to any desired degree of accuracy.

We now express the trace as a sum over a complete set of position eigenstates.

$$Z_{\rm tr} = \int dx_1 \ \langle x_1 | \ [e^{-\Delta\tau \hat{P}^2/2m} e^{-\Delta\tau m\omega^2 \hat{X}^2/2 - \Delta\tau\lambda\hat{X}^4/4}]^L \ |x_1\rangle, \qquad (3)$$

and, further, insert complete sets of eigenstates between each of the incremental time evolution operators,

$$\begin{aligned} Z_{\rm tr} \quad &= \int dx_1 dx_2 ... dx_L \langle x_1 | e^{-\Delta\tau \hat{P}^2/2m} e^{-\Delta\tau m\omega^2 \hat{X}^2/2 - \Delta\tau\lambda\hat{X}^4/4} | x_2\rangle \\ &\langle x_2 | e^{-\Delta\tau \hat{P}^2/2m} e^{-\Delta\tau m\omega^2 \hat{X}^2/2 - \Delta\tau\lambda\hat{X}^4/4} | x_3\rangle \ldots \\ &\langle x_L | e^{-\Delta\tau \hat{P}^2/2m} e^{-\Delta\tau m\omega^2 \hat{X}^2/2 - \Delta\tau\lambda\hat{X}^4/4} | x_1\rangle. \\ &= \int dx_1 dx_2 ... dx_L \exp[-\frac{1}{2} m\omega^2 \Delta\tau \sum_{l=1}^{L} x_l^2 - \frac{1}{4}\lambda\Delta\tau \sum_{l=1}^{L} x_l^4] \\ &\langle x_1 | e^{-\Delta\tau \hat{P}^2/2m} | x_2\rangle \langle x_2 | e^{-\Delta\tau \hat{P}^2/2m} | x_3\rangle \ldots \langle x_L | e^{-\Delta\tau \hat{P}^2/2m} | x_1\rangle. \quad (4) \end{aligned}$$

The position operators $\hat{X}$ have been replaced by their c-numbers eigenvalues.

Each of the remaining matrix elements in Eq. (4) can be evaluated:

$$\begin{aligned} \langle x_l | e^{-\Delta\tau \hat{P}^2/2m} | x_{l+1}\rangle \quad &= \int dp \ \langle x_l | e^{-\Delta\tau \hat{P}^2/2m} | p\rangle \langle p | x_{l+1}\rangle \\ = \int dp \ e^{-\Delta\tau p^2/2m} e^{ip(x_l - x_{l+1})} \quad &= \sqrt{\frac{2m\pi}{\Delta\tau}} e^{-\frac{1}{2} m\Delta\tau [(x_l - x_{l+1})/\Delta\tau]^2}. \quad (5) \end{aligned}$$

The momentum operators have now also disappeared in favor of c-numbers. This matrix element of the kinetic energy operator $\hat{P}^2/2m$ can be thought of as the exponential of "$\frac{1}{2}mv^2$" where the "velocity" measures the change in distance, $x_l - x_{l+1}$, between position at time slice l and $l+1$, divided by the imaginary time interval $\Delta\tau$. The prefactor of the exponential cancels when we measure expectation values. Henceforth we drop it from all equations. (This term, however, will need to be considered again in discussing measurements of the kinetic energy.)

The end result is that the partition function for our quantum problem is now expressed entirely as a multi-dimensional integral over *classical* variables,

$$\begin{aligned} Z_{\rm tr} &= \int \mathcal{D}x e^{-\Delta\tau S_{\rm cl}} \\ S_{\rm cl} &= \frac{1}{2}m\omega^2 \sum_l x_l^2 + \frac{1}{4}\lambda \sum_l x_l^4 + \frac{1}{2}m\sum_l (\frac{x_l - x_{l+1}}{\Delta\tau})^2, \end{aligned} \tag{6}$$

where we have introduced the symbol $\int \mathcal{D}x = \int dx_1 dx_2 \ldots dx_L$. The original single quantum mechanical degree of freedom $\hat{X}$ picked up an imaginary time index and became a path described by a set of classical variables x_l.

It is worth making a few general comments about the form of the classical action. $\Delta\tau S_{\rm cl}$ describes a one dimensional chain of classical oscillators tied to their equilibrium positions by anharmonic "springs" with $V(x) = \Delta\tau[\frac{1}{2}m\omega^2 x^2 + \frac{1}{4}\lambda x^4]$ and also to each other by springs of force constant $\frac{1}{2}m/\Delta\tau$. The L classical variables trace out the "world–line" in imaginary time of the single original quantum degree of freedom. The system described by Eq. 6 is also sometimes referred to as describing a set of "beads" whose positions are given by x_l, linked together to form a flexible chain or "polymer."

We can see a first example of how the paths help visualize the physics by considering the cross–over from classical to quantum behavior. Suppose we fix L. As the temperature T increases, $\beta = 1/T$ decreases, therefore so does $\Delta\tau = \beta/L$. The classical oscillators are increasingly tightly coupled since the spring constant which is the coefficient of $(x_{l+1} - x_l)^2$ is $\frac{1}{2}m/\Delta\tau$. Therefore, at high T, all the x_l will be roughly equal. The classical limit is then described by paths where the imaginary time dependence is negligible. Phrased more precisely, the x_l are constrained to be equal to a single value x, and the multi–dimensional integral reduces to a single integral, with $\Delta\tau \sum x_l \to \beta x$. One then recovers the classical partition function. We can also view this limit from fixed $\Delta\tau$. Then, if β is small, so is L, and the polymer is short and does not have much time to wiggle. In the opposite low temperature limit, the ability of the quantum paths to become extended is intimately tied to the possibility of various quantum coherence effects such as superfluidity.

We are actually not typically interested in the partition function Z itself, but rather in expectation values like the potential energy,

$$\langle \mathcal{P} \rangle = Z^{-1} {\rm Tr}\, [e^{-\beta \hat{H}} \frac{1}{2}m\omega^2 \hat{X}^2]. \tag{7}$$

We have set $\lambda = 0$ for simplicity. By the same analysis which led to Eq. 6, an approximate expression can be written as,

$$\langle \mathcal{P} \rangle_{\rm tr} = \frac{\int \mathcal{D}x \ \frac{1}{2} m\omega^2 x_1^2 \ e^{-\Delta\tau S_{\rm cl}}}{\int \mathcal{D}x \ e^{-\Delta\tau S_{\rm cl}}}. \tag{8}$$

Inspection of the form of Eq. 8 reveals that the evaluation of the quantum mechanical operator expectation value has been reduced to a ratio of classical integrals in a form identical to the one encountered in classical Monte Carlo simulation. That is, one generates configurations of the world lines $\{x_l\}$ using, for example, the Metropolis algorithm and the action $\Delta\tau S_{\rm cl}$ to make the accept–reject decision, and then accumulates a simple average of the observables in the sequence of configurations so produced. Note that one could just as well have used x_l^2 for any l in the numerator, since ${\rm Tr}[e^{-\beta\hat{H}}\hat{A}] = {\rm Tr}[e^{-(\beta-\tau)\hat{H}}\ \hat{A}\ e^{-\tau\hat{H}}]$, as a consequence of the cyclic nature of the trace. Thus the operator to be measured, $\hat{A}$, can be inserted at any point in the string of incremental imaginary time evolution operators. Indeed, one often samples all l to build up better statistics in a simulation.

It remains to determine precisely the nature of the Suzuki–Trotter approximation. For $\lambda = 0$ we can evaluate the path integral analytically, since it is a simple multi-dimensional gaussian integral.

$$Z_{\rm tr} = \int \mathcal{D}x e^{-\mathbf{x}^{\rm t} M \mathbf{x}} = \frac{\pi^{L/2}}{\sqrt{\det M}}. \tag{9}$$

Here $\mathbf{x}^{\rm t} = [x_1, x_2, \ldots x_L]$ and M is an LxL tridiagonal matrix whose only non–zero components are,

$$M_{l,l} = \frac{1}{2} m\omega^2 \Delta\tau + \frac{m}{\Delta\tau} \qquad\qquad M_{l,l\pm1} = \frac{m}{2\Delta\tau}. \tag{10}$$

The fact that the partition function is a trace makes M periodic, $M_{1,L} = M_{L,1} = \frac{m}{2\Delta\tau}$. The determinant of M is the product of its eigenvalues, which are obtained by going to momentum space. The eigenvectors of M are the vectors $\mathbf{v}_l$ with components $(\mathbf{v}_l)_n = e^{ik_l n}/\sqrt{L}$. Here $k_l = 2\pi l/L$ and $l = 1, 2, \ldots L$. The eigenvalues of M are,

$$\lambda_l = \frac{1}{2} m\omega^2 \Delta\tau + \frac{m}{\Delta\tau}[1 - \cos(k_l)], \tag{11}$$

and the determinant, $\det M = \prod_l \lambda_l$.

An expectation value like that of the potential energy, and more general "correlation functions" in imaginary time, can be evaluated by recalling the identity,

$$\langle x_l x_n \rangle = Z_{\rm tr}^{-1} \int \mathcal{D}x \, x_l x_n e^{-\mathbf{x}^{\rm t} M \mathbf{x}} = \frac{1}{2} G_{ln}, \tag{12}$$

where $G = M^{-1}$. Thus for example,

$$\begin{aligned} \langle \mathcal{P} \rangle_{\rm tr} &= \frac{1}{2} m\omega^2 \langle x_l^2 \rangle = \frac{1}{4} m\omega^2 G_{ll} \\ &= \frac{1}{4L} m\omega^2 \, {\rm Tr}\, G = \frac{1}{4L} m\omega^2 \sum_l \frac{1}{\lambda_l}, \end{aligned} \tag{13}$$

where we used the translation invariance of M (and G) to write $G_{ll} = (1/L){\rm Tr}\, G$. Eq. 13 gives an analytic expression for the Trotter approximation for the potential energy. The exact result is, of course,

$$P = \frac{1}{2}\omega(\frac{1}{e^{\beta\omega} - 1} + \frac{1}{2}). \tag{14}$$

Before we present a comparison of Eqs. 13 and 14, we make a few comments about the matrix eigenspectrum of M and its relation to simulations. The "condition number," the ratio of largest to smallest eigenvalue, of the matrix M becomes increasingly large as $\Delta\tau$ decreases. For $\Delta\tau$ small, $\lambda_{\rm max} = \lambda_{L/2} \approx 2m/\Delta\tau$ and $\lambda_{\rm min} = \lambda_L = \frac{1}{2} m\omega^2 \Delta\tau$, so that $\lambda_{\rm max}/\lambda_{\rm min} \approx 4/\omega^2\Delta\tau^2$. Large condition number is generally associated with difficulties in doing numerical work, and Monte Carlo is no exception. Here the problem manifests itself as long autocorrelation times. (See Fig. 1.) If we suggest a move of a single coordinate x_l it will not be very likely to be accepted unless the change is small, since otherwise we will be stretching the springs to the neighboring beads too much, at a great cost in energy. Yet such small changes are ineffective at generating the large displacements characteristic of the low frequency modes. This is a very simple example of the class of problems addressed by Fourier acceleration[9] and loop algorithms. The solution in this case is immediately evident: If we change variables to normal mode coordinates, then we can use different step sizes for the different modes, allowing efficient equilibration.

In practice, if we want to measure some observable as a function of temperature, the best approach is to fix $\Delta\tau$ to be some "small" value and change β by changing L. The reason is that the Trotter errors can be roughly estimated as $\Delta\tau^2 E_1 E_2$, where E_1 and E_2 are energy scales in H_1 and H_2, since this is the size of the commutator which is disregarded in breaking up the exponential. Thus, crudely speaking, $\Delta\tau$ must be chosen to make $\Delta\tau^2 E_1 E_2$ "small," a condition which is independent of β. The results of such a calculation are shown in Fig. 2. We have chosen $m = \omega = 1$. Note that even for $\Delta\tau = 0.25$ the results for the potential energy are almost indistinguishable from the exact result.

It is hard to discern the systematic error in the scales used in Fig. 2. We plot the difference between the exact and approximate results in Fig. 3. Although in this case the Trotter errors are analytically calculable, in most

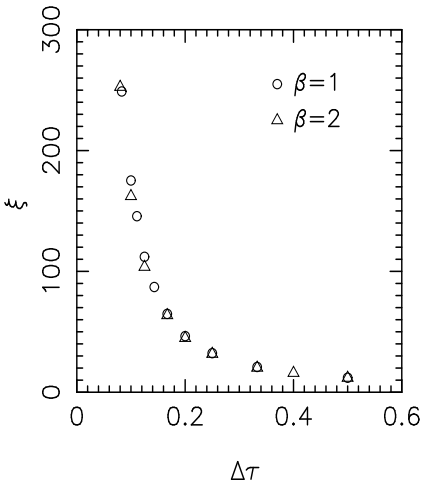

Figure 1. Autocorrelation time ξ of a world–line simulation of the quantum harmonic oscillator. ξ is defined as the time it takes the normalized correlation of the deviation of a phonon displacement from its average value at two different Monte Carlo times to fall to $1/e$. We have chosen $m = \omega = 1$. Also, the scale of the size of suggested moves is chosen to be $A = 1.0$, where the suggested shift in each $x(l)$ is given by $dx = A * (r - \frac{1}{2})$ and r is a random number which is uniform on $[0, 1]$.

cases the determination of the optimal $\Delta\tau$ is empirical. The choice is based on a compromise between the reduction of systematic errors at small $\Delta\tau$ and the accompanying increase in computational expense. Often, extrapolation is useful, since it allows simulations at relatively large $\Delta\tau$ to yield results at the desired $\Delta\tau \to 0$.

We can ask about the analytic form of the Trotter corrections. It has been shown[7] that under very general conditions (for example the observable being measured must be Hermitian) the leading corrections are second order in $\Delta\tau$. This is explicitly illustrated in Fig. 4 where we show a comparison of the exact finite $\Delta\tau$ form of Eq. 13 with the exact $\Delta\tau = 0$ form Eq. 14.

In principle, one could also sweep temperature by fixing L and changing $\Delta\tau$. However, at low temperatures $\Delta\tau$ will grow large, and the systematic errors will vary with T. The result of such a procedure is shown in Fig. 5. There is an interesting cross–over from behavior characteristic of the original quantum Hamiltonian to some other effective large $\Delta\tau$ model. This behavior is revealed especially clearly in the specific heat $C = dE/dT$

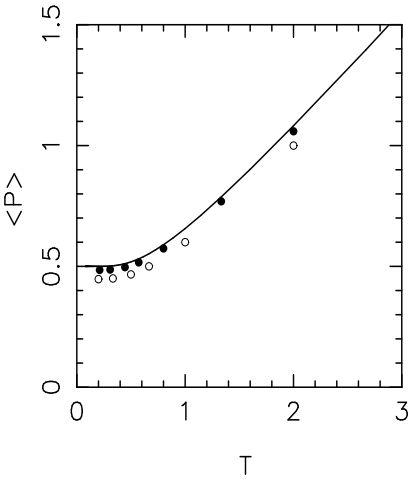

Figure 2. The potential energy of a single Quantum Oscillator as a function of temperature. Here $m = 1$ and $\omega = 2$. The full line is the exact result while the open and closed circles are for finite $\Delta\tau = 0.50$ and $\Delta\tau = 0.25$ respectively.

which exhibits an anomalous peak when $\Delta\tau$ becomes too large.

The kinetic energy can also be measured. The desired trace $\mathrm{Tr}\hat{P}^2 e^{-\beta\hat{H}}$ differs from the partition function in the single matrix element,

$$\begin{aligned}
\langle x_1|\hat{P}^2 e^{-\Delta\tau\hat{P}^2/2m}|x_2\rangle &= \int dp \langle x_1|p\rangle\langle p|\hat{P}^2 e^{-\Delta\tau\hat{P}^2/2m}|x_2\rangle \\
&= \int dp\, p^2 e^{-\Delta\tau p^2/2m} e^{ip(x_1-x_2)} \\
&= -2m\frac{\partial}{\partial\Delta\tau}\int dp\, e^{-\Delta\tau p^2/2m} e^{ip(x_1-x_2)}. \qquad (15)
\end{aligned}$$

The last integral is given by Eq. 5. The derivative with respect to $\Delta\tau$ yields two terms, and the estimator for the kinetic energy is

$$\frac{1}{2\Delta\tau} - \langle\frac{1}{2}m(\frac{x_2-x_1}{\Delta\tau})^2\rangle \qquad (16)$$

There are two interesting features in this expression. First, the counter-intuitive minus sign in front of the "expected" velocity–like term can be understood as a consequence of the fact that we are working in imaginary time. But notice that even beyond the minus sign, the velocity term which

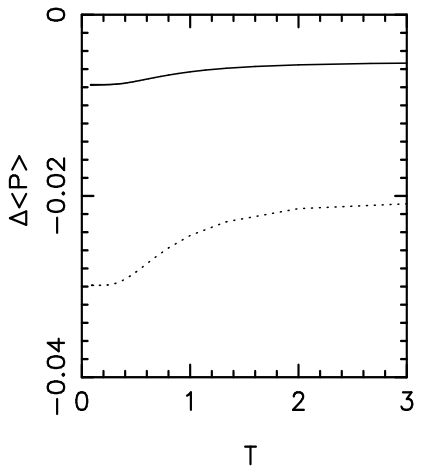

Figure 3. Relative error between exact and approximate results for the potential energy of a single Quantum Oscillator as a function of temperature. Here $m = 1$ and $\omega = 2$. The dotted and full lines are for finite $\Delta\tau = 0.25$ and $\Delta\tau = 0.125$ respectively.

one naively might have thought to be the estimator, contains both the correct answer and a large negative contribution which diverges as $\Delta\tau \to 0$, cancelling the first term. The expectation values in Eq. 16 can, of course, be rewritten in terms of the Green's function elements G_{12} and G_{11}. Finally, we comment that the virial theorem, is obeyed even in the presence of Trotter errors. That is, the expressions Eqs. 13,15 for the kinetic and potential energies give the same numeric result even at finite $\Delta\tau$.

Once the path integral for the single quantum oscillator is written, the effective classical action for much more complicated models can be obtained immediately. For example, the path integral action for an arbitrary potential,

$$\hat{H} = \frac{\hat{P}^2}{2m} + V(\hat{X}), \tag{17}$$

is,

$$S_{\rm cl} = \sum_l V(x_l) + \frac{1}{2} m \sum_l (\frac{x_l - x_{l+1}}{\Delta\tau})^2. \tag{18}$$

This illustrates an important feature of QMC: Changes in the Hamiltonian often translate into straightforward modifications of the underlying simulation code, whereas analytic approaches may need to be entirely reformu-

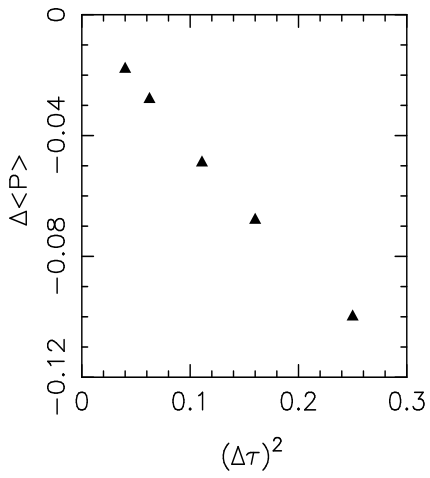

Figure 4. The quadratic in $\Delta\tau$ nature of the Trotter errors is illustrated by showing the potential energy at fixed $\beta = 2$ as a function of $(\Delta\tau)^2$. Here $m = 1$ and $\omega = 2$.

lated. This simple problem also already exhibits one of the crucial features of the world–line algorithm: Changes to the potential energy (terms that are diagonal in the basis of intermediate states) are the ones that are trivial to make in the code. As we shall see, changes to the kinetic energy are more difficult to incorporate in general. Conversely, changes to the form of the kinetic energy are easy to make in determinant codes, while increased complexity in interactions is much more difficult.

A more interesting example of generalizing world–line codes is to consider the problem of writing down the path integral for the Hamiltonian of a one dimensional chain of coupled quantum harmonic oscillators,

$$\hat{H} = \sum_n [\frac{\hat{P}_n^2}{2m} + \frac{1}{2} m\omega^2 \hat{X}_n^2] + \frac{1}{2}\alpha \sum_n (\hat{X}_n - \hat{X}_{n+1})^2. \tag{19}$$

Here the index n labels the different quantum degrees of freedom. The associated classical action is,

$$\begin{aligned} S_{\rm cl} &= \frac{1}{2} m\omega^2 \sum_{nl} x_{n,l}^2 + \frac{1}{2} m \sum_{nl} (\frac{x_{n,l} - x_{n,l+1}}{\Delta\tau})^2 \\ &+ \frac{1}{2}\alpha \sum_{nl} (x_{n,l} - x_{n+1,l})^2. \end{aligned} \tag{20}$$

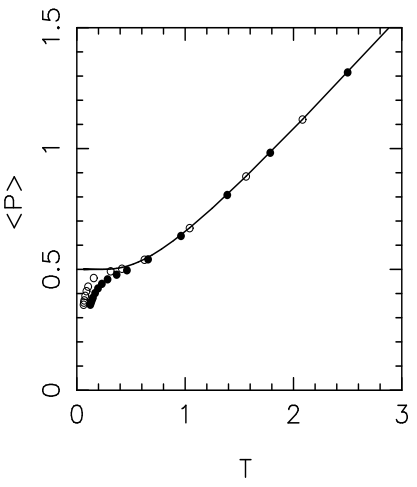

Figure 5. The potential energy of a single Quantum Oscillator as a function of temperature. Here $m = 1$ and $\omega = 2$. The full line is the exact result for $\Delta\tau = 0$ while the closed and open circles are for fixed $L = 8$ and $L = 16$ respectively.

The quantum mechanical operators $\hat{X}_n$ generate a set of classical variables $x_{n,l}$ with an additional imaginary time index. Thus the partition function of the one dimensional quantum problem maps onto a classical problem in $1 + 1$ dimensions. Anisotropic couplings distinguish correlations in space and imaginary time.

3. The One–Dimensional Ising Model in a Transverse Field

In the previous section we described the world–line approach for a single quantum oscillator and collections of quantum oscillators. These models provide the most simple illustration of the technique, and are also solvable analytically, in the absence of anharmonicity. The bulk of the applications of the world–line approach, however, has been to quantum spins and interacting bosons and fermions. In this section we will describe the Ising model in a transverse magnetic field. Here, the effective classical model is especially simple, and, in fact, the world–line mapping allows us to determine much of the physics even before performing simulations. This model, with the addition of randomness to the couplings, has revealed some remarkable features of disordered quantum systems, partially through numerical work.[10, 11]

The Ising model provides a simple description of magnetic phase transitions. Classical "spin" degrees of freedom $S_{\mathbf{i}}^z$ which can take on the values $S_{\mathbf{i}}^z = \pm 1$ exist on the sites $\mathbf{i}$ of a lattice. Spins on different lattice sites interact via a coupling constant J,

$$H_0 = J \sum_{\langle \mathbf{ij} \rangle} S_{\mathbf{i}}^z S_{\mathbf{j}}^z. \tag{21}$$

The symbol $\langle \mathbf{ij} \rangle$ indicates a sum over near–neighbor sites, the case most often considered. For a ferromagnetic coupling $J < 0$, spins $S_{\mathbf{i}}^z$ and $S_{\mathbf{j}}^z$ with the same value have lower energy and hence order is favored. On the other hand, the entropy favors random spin configurations. This model has a finite temperature phase transition in two and higher dimensions in which the global up–down symmetry of the spins is broken and a non–zero spontaneous magnetization $m = \langle S_{\mathbf{i}}^z \rangle$ exists below the critical temperature T_c. For a two–dimensional square lattice in which the couplings J_x and J_y between neighbors in the x and y directions are identical, $T_c \approx 2.269J$. More generally, if J_x and J_y differ, T_c is given by

$$2\tanh[\frac{2J_x}{kT_c}]\tanh[\frac{2J_y}{kT_c}] = 1. \tag{22}$$

The Ising model Eq. 22 has been very extensively studied by classical monte carlo methods.[12] However, if a *transverse* magnetic field, $H_1 = -B \sum_{\mathbf{i}} S_{\mathbf{i}}^x$, is added, quantum simulation methods must be employed owing to the non–commutivity of the operators. We proceed as for the quantum harmonic oscillator, beginning with the partition function, discretizing the inverse temperature β, and separating the two non–commuting pieces of the Hamiltonian.

$$Z = \mathrm{Tr} e^{-\beta \hat{H}} = \mathrm{Tr}[e^{-\Delta\tau \hat{H}}]^L \approx Z_{\mathrm{tr}} = \mathrm{Tr}[e^{-\Delta\tau \hat{H}_0} e^{-\Delta\tau \hat{H}_1}]^L. \tag{23}$$

Complete sets of states $|S_1^z \, S_2^z \ldots S_N^z\rangle$ which are eigenstates of the z component of spin on each of the N sites of the spatial lattice are then inserted.

$$\begin{aligned} Z \approx \sum_{S_{\mathbf{i}l}^z} \quad & \langle S_{11}^z S_{21}^z \ldots S_{N1}^z | e^{-\Delta\tau H_0} e^{-\Delta\tau H_1} | S_{12}^z S_{22}^z \ldots S_{N2}^z \rangle \\ & \langle S_{12}^z S_{22}^z \ldots S_{N2}^z | e^{-\Delta\tau H_0} e^{-\Delta\tau H_1} | S_{13}^z S_{23}^z \ldots S_{N3}^z \rangle \ldots \\ & \langle S_{1L}^z S_{2L}^z \ldots S_{NL}^z | e^{-\Delta\tau H_0} e^{-\Delta\tau H_1} | S_{11}^z S_{21}^z \ldots S_{N1}^z \rangle. \end{aligned} \tag{24}$$

The eigenvalues $S_{\mathbf{i}l}^z$ have a second label l to specify the imaginary time slice. Like the potential energy operator in our quantum oscillator example, the

operator $\exp(-\Delta\tau H_0)$ is diagonal in the basis chosen for the intermediate states, and immediately comes out of the expectation values.

$$\begin{aligned} Z \approx \quad & \sum_{S^z_{\mathbf{i}l}} \exp[J\Delta\tau \sum_{\langle \mathbf{ij}\rangle, l} S^z_{\mathbf{i}l} S^z_{\mathbf{j}l}] \, \langle S^z_{11} S^z_{21} \ldots S^z_{N1} | e^{-\Delta\tau \hat{H}_1} | S^z_{12} S^z_{22} \ldots S^z_{N2} \rangle \\ & \langle \; S^z_{12} S^z_{22} \ldots S^z_{N2} | e^{-\Delta\tau \hat{H}_1} | S^z_{13} S^z_{23} \ldots S^z_{N3} \rangle \ldots \\ & \langle \; S^z_{1L} S^z_{2L} \ldots S^z_{NL} | e^{-\Delta\tau \hat{H}_1} | S^z_{11} S^z_{21} \ldots S^z_{N1} \rangle \end{aligned} \tag{25}$$

The remaining expectation values of the operators of x component of spin are easily evaluated, since $\hat{H}_1$ is the sum of pieces which commute. Each matrix element factorizes,

$$\begin{aligned} & \langle S^z_{1l} S^z_{2l} \ldots S^z_{Nl} | e^{-\Delta\tau \hat{H}_1} | S^z_{1,l+1} S^z_{2,l+1} \ldots S^z_{N,l+1} \rangle \\ & \qquad = \prod_{\mathbf{i}} \langle S^z_{\mathbf{i},l} | e^{\Delta\tau B S^x_{\mathbf{i}}} | S^z_{\mathbf{i},l+1} \rangle . \end{aligned} \tag{26}$$

These single site matrix elements are,

$$\langle S^z_{\mathbf{i}l} | e^{\Delta\tau B S^x_{\mathbf{i}}} | S^z_{\mathbf{i}l+1} \rangle = e^{-\lambda S^z_{\mathbf{i}l} S^z_{\mathbf{i}l+1}} , \tag{27}$$

where $\lambda = -\frac{1}{2}\ln[\tanh\Delta\tau B]$. Thus the effect of the transverse magnetic field is to introduce an Ising–like coupling in the imaginary time direction. This is in close analogy to the kinetic energy operator in the quantum oscillator case, which coupled positions at different imaginary times.

With the matrix elements evaluated, we have,

$$Z_{\rm tr} = \sum_{S^z_{\mathbf{i}l}} e^{-E} \tag{28}$$

$$E = -J\Delta\tau \sum_{\langle \mathbf{ij}\rangle, l} S^z_{\mathbf{i}l} S^z_{\mathbf{j}l} - \lambda \sum_{\mathbf{i},l} S^z_{\mathbf{i}l} S^z_{\mathbf{i}l+1}, \tag{29}$$

which is identical to that of a $(d+1)$–dimensional classical Ising model with one direction having a different coupling constant, λ, from the other d dimensions, $J\Delta\tau$.

We can now infer the phase diagram of the quantum model in d dimensions from what is known concerning the classical model in $d+1$ dimensions. Consider, for example, the case of a one–dimensional Ising model in a transverse field. The mapping to the two–dimensional anisotropic classical model tells us there is a phase transition in the J–B plane whose boundary is given by Eq. 22, namely, $2\tanh[2J\Delta\tau]\tanh[2\lambda] = 1$. This curve separates a small B ferromagnetic phase, in which there is a symmetry–breaking spontaneous magnetization in the z direction, from a paramagnetic phase at larger B.

It is important to distinguish the role of β in the original quantum model and its classical analog. The classical model exhibits a phase transition *in the thermodynamic limit*, that is, when the size of the lattice is infinite, and when βJ_x and βJ_y satisfy Eq. 22. In the language of the one–dimensional Ising model in a transverse field, the condition that the classical lattice be infinite corresponds to taking $\beta \to \infty$, since β gives one of the classical linear dimensions. $N \to \infty$ is also required of the original linear lattice size. In other words, there is a "quantum phase transition" in the *ground state* of the one–dimensional Ising model in a transverse field as a function of the parameters J and B.

Besides predicting a phase transition and giving an analytic expression for the phase boundary, the mapping also tells us the dynamic critical exponent z, which defines the relationship between the correlation length in the spatial and imaginary time directions near the critical point. (See also section 7.) Since the mapping is to a classical model which, to within an anisotropy in coupling constants, looks the same in these directions, we infer that $z = 1$ for the Ising model in a transverse field (in any dimension). In the Hamiltonians to be discussed in the following sections, the structure of the action will be rather different in the space and imaginary time directions, so that one might expect $z \neq 1$. We will briefly discuss the implications of the value of z for finite size scaling in Section 7.

We conclude this section by noting that the problem of a one–dimensional Ising model in a *random* transverse magnetic field has recently revealed a number of fascinating features.[10, 11] None of the steps in the above discussion of the world–line formulation required that the field B is site independent, or that the coupling constant J not depend on the link **ij**. World–line simulations of the disordered model[13] are then a simple generalization of the clean case, again illustrating the powerful feature of these simulations that new Hamiltonians and their associated physics can often be explored with simple modifications of codes.

4. The Spin–1/2 XXZ Hamiltonian

In the preceding section we saw how a d–dimensional Ising model in a transverse magnetic field maps onto an anisotropic $d+1$–dimensional classical Ising model. The quantum mechanical Hamiltonian had a simple classical analog because the non–diagonal terms in the Hamiltonian appeared only as single site operators. We now turn to Hamiltonians where the non–diagonal terms appear in pairs. As we shall see, this results in more complicated effective actions and restrictions on the allowed spin patterns.

Consider the quantum XXZ Hamiltonian,

$$\begin{aligned} H &= \sum_{\langle \mathbf{ij} \rangle} J_x (S^x_{\mathbf{i}} S^x_{\mathbf{j}} + S^y_{\mathbf{i}} S^y_{\mathbf{j}}) + J_z S^z_{\mathbf{i}} S^z_{\mathbf{j}} - B \sum_{\mathbf{i}} S^z_{\mathbf{i}} \\ &= \sum_{\langle \mathbf{ij} \rangle} \frac{J_x}{2} (S^+_{\mathbf{i}} S^-_{\mathbf{j}} + S^-_{\mathbf{i}} S^+_{\mathbf{j}}) + J_z S^z_{\mathbf{i}} S^z_{\mathbf{j}} - B \sum_{\mathbf{i}} S^z_{\mathbf{i}} \end{aligned} \tag{30}$$

Here $S^x_{\mathbf{i}}, S^y_{\mathbf{i}}$ and $S^z_{\mathbf{i}}$ are quantum spin–1/2 operators at each site $\mathbf{i}$, and $S^+_{\mathbf{i}}, S^-_{\mathbf{i}}$ are the associated raising and lowering operators. When $J_z > J_x$ this model is in the Ising universality class and exhibits a finite temperature phase transition in zero field to a state with long range order, in dimensions greater than $d = 1$. For $J_x > J_z$, the model is in the XY universality class, again with a finite temperature phase transition in zero field to a state with long range order in dimensions greater than $d = 2$, with a Kosterlitz–Thouless phase transition to a state with spin correlations which decay with a power–law in $d = 2$. The isotropic Heisenberg point $J_x = J_z$ has long range order in $d = 2$ only at $T = 0$.[14] As we shall see in the following section, this spin–1/2 XXZ Hamiltonian is isomorphic to a lattice system of hard–core bosons with a near neighbor interaction.

We formulate a world–line simulation by discretizing $\beta = L\Delta\tau$ in the partition function. However, the division of the Hamiltonian introduces a new feature. The principle governing how to divide H into pieces is that it must be possible to evaluate the matrix elements which arise after the introduction of complete sets of states. A convenient choice in the case of the XXZ Hamiltonian is the "checkerboard" decomposition.[15] For simplicity, consider the case of one–dimension. We divide $H = H_1 + H_2$ where,

$$\begin{aligned} H_1 &= \sum_{i \text{ odd}} \frac{J_x}{2} (S^+_i S^-_{i+1} + S^-_i S^+_{i+1}) + \frac{J_z}{2} S^z_i S^z_{i+1} - \frac{B}{2} (S^z_i + S^z_{i+1}) \\ H_2 &= \sum_{i \text{ even}} \frac{J_x}{2} (S^+_i S^-_{i+1} + S^-_i S^+_{i+1}) + \frac{J_z}{2} S^z_i S^z_{i+1} - \frac{B}{2} (S^z_i + S^z_{i+1}). \end{aligned} \tag{31}$$

This is illustrated in Fig. 6. We will now discuss why this is a useful division.

The expression which arises for the path–integral for the partition function, after the introduction of a complete set of states which are diagonal in the z component of spin, is,

$$\begin{aligned} Z &= \sum_{S^z_{il}} \exp[-J_z \Delta\tau \sum_{i,l} S^z_{i,l} S^z_{i+1,l} - B\Delta\tau \sum_{i,l} S^z_{i,l}] \\ &\langle \; S^z_{11} S^z_{21} \ldots S^z_{N1} | e^{-\hat{h}} | S^z_{12} S^z_{22} \ldots S^z_{N2} \rangle \\ &\langle \; S^z_{12} S^z_{22} \ldots S^z_{N2} | e^{-\hat{h}} | S^z_{13} S^z_{23} \ldots S^z_{N3} \rangle \ldots \\ &\langle \; S^z_{1,2L} S^z_{2,2L} \ldots S^z_{N,2L} | e^{-\hat{h}} | S^z_{11} S^z_{21} \ldots S^z_{N1} \rangle, \end{aligned} \tag{32}$$

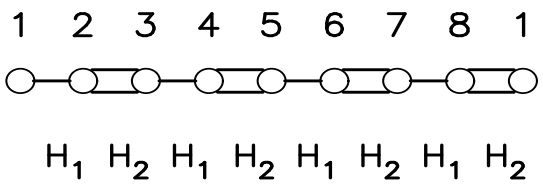

Figure 6. The division of the one–dimensional XXZ Hamiltonian into H_1 and H_2, each of which consists of independent two–site pieces. Periodic boundary conditions in the spatial direction connect the last site, $x = 8$ to the first, $x = 1$.

with the abbreviation $\hat{h}$ for the xy terms in the Hamiltonian. We have to introduce $2L$ time slices in this checkerboard decomposition in one dimension, because neither H_1 nor H_2 is diagonal in the basis of intermediate states chosen.

The crucial observation is that H_1 and H_2 consist of independent two–site pieces. Thus the matrix elements factorize,

$$\begin{aligned} &\langle S^z_{1l} S^z_{2l} \ldots S^z_{Nl} | e^{-\hat{h}} | S^z_{1,l+1} S^z_{2,l+1} \ldots S^z_{N,l+1} \rangle \\ &\quad = \prod_{i \text{ odd}} \langle S^z_{i,l} S^z_{i+1,l} | e^{-\hat{h}_i} | S^z_{i,l+1} S^z_{i+1,l+1} \rangle, \end{aligned} \tag{33}$$

and one must only evaluate the corresponding two site expectation values. The results are,

$$\begin{aligned} \langle + + |e^{-\hat{h}_i}| + + \rangle &= \langle - - |e^{-\hat{h}_i}| - - \rangle = 1, \\ \langle + - |e^{-\hat{h}_i}| + - \rangle &= \langle - + |e^{-\hat{h}_i}| - + \rangle = \cosh(\frac{J_x}{2}\Delta\tau), \\ \langle + - |e^{-\hat{h}_i}| - + \rangle &= \langle - + |e^{-\hat{h}_i}| + - \rangle = -\sinh(\frac{J_x}{2}\Delta\tau), \end{aligned} \tag{34}$$

with all other matrix elements zero. Note that the only non–zero matrix elements are those between states which have the same $S^z_{\rm tot} = S^z_1 + S^z_2$ in the two time slices. This is a consequence of the fact that $[\hat{h}, S^z_{\rm tot}] = 0$.

The off–diagonal matrix elements are negative if the XY coupling is *antiferromagnetic*, $J_x > 0$. This is an instance of the "sign problem" in quantum monte carlo. If the XY coupling is ferromagnetic, $J_x < 0$, then there is no sign problem. In the case of a near–neighbor antiferromagnetic coupling on a bipartite lattice, we can eliminate the sign problem by rotating the spin operators on one sublattice. This changes the sign of J_x and the world–line simulation is applicable, but does not alter the physics since it simply corresponds to a different choice of direction of the local axes of spin

quantization. If the signs cannot be eliminated by such a rotation or some other means, then the world–line method will not work for the Hamiltonian in question. Examples of such cases are antiferromagnetic models on non–bipartite lattices like the triangular lattice, or models with longer range antiferromagnetic coupling, such as the two–dimensional, square lattice, "J_1–J_2" Heisenberg model which has a next near–neighbor antiferromagnetic coupling J_2 across the diagonal of a square. This sign problem is the most fundamental limitation to quantum simulation techniques. It arises not only in the world–line algorithm, but also in the determinant approach, in ground state projection methods, etc.

In the absence of a sign problem the simulation can be implemented. It is useful to picture the structure of the checkerboard break–up by drawing the (1+1)–dimensional array of spins and shading the squares corresponding to bonds across which a piece of the Hamiltonian acts. Thus H_1 connects spatial sites $(1,2)$, $(3,4)$, $\ldots(N-1,N)$ from time slice l to $l+1$ where l is odd, and likewise H_2 connects spatial sites $(2,3)$, $(4,5)$, $\ldots(N,1)$ from time slice l to $l+1$ where l is even. (The last pair $(N,1)$ is present if we have periodic boundary conditions which connect the first and last sites in our Hamiltonian.) The resulting "checkerboard lattice" is illustrated in Fig. 7.

That the matrix elements vanish unless the sum of the z components of spin at the top and bottom of a shaded square are equal puts constraints on the terms in the sum over $S^z_{\mathbf{i}l}$ which contribute to the partition function. These conservation laws can best be visualized as follows: Draw lines connecting the sites on which the z component of spin is pointed up. Since the number of such up spin sites is conserved from time slice to time slice, the result is a set of continuous "world–lines". The world–lines can cross only the shaded squares of the checkerboard lattice, since it is on these that the Hamiltonian acts. The periodic boundary conditions inherent in the trace require that these world–lines also connect continuously from the last time slice, $l = 2L$, to the first, $l = 1$. As we shall see, this same construction occurs in the monte carlo path integral formulation for problems of interacting bosons and fermions where the conservation law is particle number, and the name "world–line" is especially appropriate.

We need to formulate monte carlo moves which respect the restricted class of spin configurations which is allowed. A move which flips a single spin $S^z_{\mathbf{i}l} \to -S^z_{\mathbf{i}l}$ would always give rise to zero matrix elements if the original configuration had non–zero Boltzmann weight. Put differently, it would "break" a world–line. It is easy to see (Fig. 7) that moves which "pull" a world–line across an *unshaded* square of the checkerboard lattice preserve all the local conservation laws and result in configurations of nonzero weight, assuming the original configuration was allowed. Four spin variables are changed in such an update, and the values of the matrix elements on four of

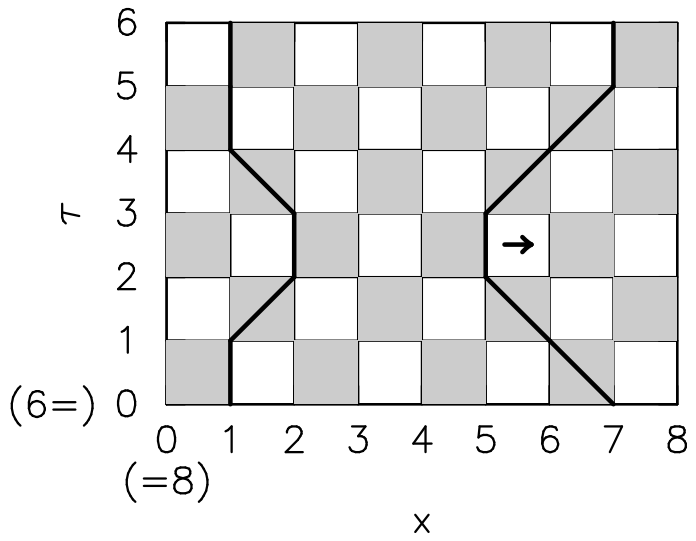

Figure 7. The "checkerboard" which arises by shading those plaquettes of the space–imaginary time lattice across which time evolution operators act. In the figure, the number of spatial sites $N = 8$ and $L = 3$. In one dimension, the number of imaginary time slices τ in the checkerboard lattice is twice L, since H_1 and H_2 both have to act. The periodic boundary conditions connect sites and slices at the edges of the lattice, illustrated here by the identification of the boundaries $x = 0$ and $\tau = 0$ with $x = 8$ and $\tau = 6$ respectively. World lines can traverse only diagonals of shaded squares. A typical monte carlo move which pulls a world–line across an unshaded square is shown.

the plaquettes are modified. This means that the decision making process is local, and updating all the degrees of freedom on the lattice scales linearly with the lattice size. An acceptance–rejection step using the Metropolis algorithm in which the move is accepted with probability $\max(1,R)$, where R is the ratio of the product of new to old values of the matrix elements on the four modified plaquettes, satisfies detailed balance, and will generate spin configurations with Boltzmann weight equal to the product of all the matrix elements.

This world–line algorithm for one–dimensional quantum spin–1/2 systems can easily be generalized to higher dimension. There are different possibilities for dividing up the Hamiltonian. For $d = 2$, one might break H into four pieces corresponding to odd and even links in each of the x and y directions of the spatial lattice. This requires $4L$ intermediate states, where $L = \beta/\Delta\tau$. The allowed spin configurations are even more restricted, and not completely trivial to visualize. Pulling world–lines across an unshaded plaquette in either the x or y directions are still allowed moves. These will now change the values of eight spins and eight of the plaquettes of the lattice. However, these moves do not exhaust the full phase space. Moves

which introduce a local twist of the lines are also permitted, and should be included to ensure ergodicity. Indeed, the density of these local twists has been used to characterize the various phases of the Hamiltonian.[16]

It is also possible to break H into only two pieces, each consisting of independent four site terms. The resulting matrix elements are a bit more complicated to evaluate, but the variance in the QMC is reduced since more of the sum is done analytically. Also, this approach involves introducing only half as many time slices ($2L$), and provides an easier means to keep track of local twists.

It is possible to introduce variance reduction techniques into world–line monte carlo. Rather than suggesting a move which would pull a line across an unshaded plaquette each time that plaquette is encountered in sweeping through the lattice, one can modify the suggestion probability based on the configuration of spins on neighboring sites. In general this is done according to some insight into the expected correlations, reducing the rate of suggestion of moves whose acceptance would violate expected structures. Of course, any such modification of the suggestion probability must also be appropriately accounted for in the Metropolis acceptance/rejection step so as to preserve detailed balance. Thus the algorithm always remains exact, to within Trotter errors, and only the variance and equilibration are affected.[1]

The cpu time scaling of a single sweep through the lattice in the world–line algorithm is linear in both the spatial size N and the inverse temperature $L = \beta/\Delta\tau$, because the Metropolis decision–making step involves only the evaluation of a local quantity, the ratio of a product of matrix elements for the small number of plaquettes whose spin configuration was changed. This is in contrast to the "determinant" QMC algorithm described in chapter 7 which has a spatially nonlocal action resulting in a N^3L scaling.[17] However, we should emphasize that this nominally linear scaling is quite misleading. World–line simulations can have enormous equilibration and autocorrelation times, for example, easily 10^4 sweeps on a "typical" N=8x8 spatial and $L = 80$ time slice lattice. This is what has motivated the development of loop algorithms.[3]

Snapshots of the spin configurations in the course of the simulation of the XXZ Hamiltonian are given in Fig. 8 for $J_x = 1$ and $J_z = 0, 1, 2$. These provide intuitive pictures of the underlying correlations. For example, we can see the antiferromagnetic spin order in the z direction build up as J_z increases.

While, these snapshots provide qualitative pictures of the physics, we need to describe how to measure operator expectation values. It turns out there are severe limitations to what one can calculate. This is a serious drawback of the world–line algorithm, especially in comparison with the de-

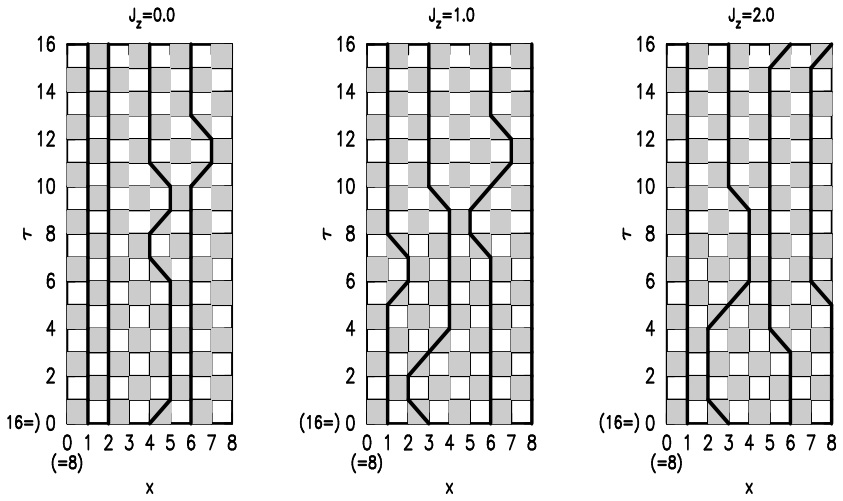

Figure 8. "Typical" snapshots of world–line configurations for the XXZ Hamiltonian on an $N = 8$ site lattices at $J_z/J_x = 0, 1, 2$, inverse temperature $\beta = 2$ (with $L = 8$), and magnetization $M_z = 0$. The world–lines follow the trajectories of the up spins, as described in the text. As J_z/J_x becomes larger the world–lines increasingly tend to occupy every other spatial site, reflecting a growth of antiferromagnetic order.

terminant approach where any equal time measurement can be constructed from the quantities used in updating the auxiliary field.[2] Consider evaluating,

$$\langle \hat{A} \rangle = Z^{-1} \mathrm{Tr}[\hat{A} e^{-\beta \hat{H}}]. \tag{35}$$

If the operator $\hat{A}$ is diagonal in the basis of complete sets of intermediate states, the procedure is simple. $\hat{A}$ acts on the state $\langle S^z_{11} S^z_{21} \ldots S^z_{N1}|$ yielding a number $a[S^z_{11}, S^z_{21}, \ldots S^z_{N1}]$ without altering the state. The operator $e^{-\beta \hat{H}}$ then generates in the numerator the same sequence of matrix elements as in the partition function in the denominator. Thus if configurations are generated according to this product of matrix elements, one simply accumulates the numbers $a[S^z_{11} S^z_2 \ldots S^z_{N1}]$ and averages them over the course of the measurement sweeps in the simulation. As described in section 2, the periodic nature of the trace allows the operator $\hat{A}$ to be inserted at any point in the string of matrix elements. To improve statistics, one can measure values $a[S^z_{1l}, S^z_{2l}, \ldots S^z_{Nl}]$ on any time slice l.

Expectation values of diagonal operators $\hat{A}(0)\hat{B}(\tau)$ which are offset in imaginary time (here $\hat{B}(\tau) = e^{\tau \hat{H}} \hat{B} e^{-\tau \hat{H}}$) can also be measured for

$\tau = n\Delta\tau$ by inserting $\hat{A}$ and $\hat{B}$ into positions in the product of matrix elements separated by imaginary time τ and accumulating the numbers $a[\, S^z_{1l},\, S^z_{2l},\, \ldots S^z_{Nl}]\; b[\, S^z_{1,l+n},\, S^z_{2,l+n},\, \ldots S^z_{N,l+n}]$ which arise. Again we can improve statistics by inserting the pair A, B anywhere in the string of incremental time evolution operators as long as they are separated by imaginary time $n\Delta\tau$.

Measuring matrix elements of operators which are not diagonal in the basis of intermediate states is harder, and, indeed, often not possible. Consider $\langle S^+_i S^-_{i+1} + S^-_i S^+_{i+1}\rangle$, an expectation value which is needed in determining the energy. This operator acts on an intermediate state vector and modifies it, so that the matrix elements in the numerator and denominator are no longer identical. This means that our ratio of integrals is no longer of the form of an integral of some "weight function" in the denominator and the product of the same weight function and a "measurement" in the numerator. We can fix this by multiplying and dividing by the matrix element in the denominator which is missing in the numerator. Then the same product appears in both places, and the measurement is made by accumulating the ratio of the new matrix element to the old one. That is,

$$\langle S^+_i S^-_{i+1} + S^-_i S^+_{i+1}\rangle = \left\langle \frac{\langle\, S^z_{i,l}\, S^z_{i+1,l}|(S^+_i S^-_{i+1} + S^-_i S^+_{i+1})e^{-\Delta\tau \hat{H}_j}|\, S^z_{i,l+1}\, S^z_{i+1,l+1}\rangle}{\langle\, S^z_{i,l}\, S^z_{i+1,l}|e^{-\Delta\tau \hat{H}_j}|\, S^z_{i,l+1}\, S^z_{i+1,l+1}\rangle} \right\rangle_{\rm MC}. \quad (36)$$

where $\langle\ \rangle_{\rm MC}$ denotes a monte carlo average of the indicated ratio of matrix elements. We have again exploited the fact that the operator can be inserted at any point l in the string of intermediate states. H_j is whatever piece of the Hamiltonian happens to be acting at that point. In fact, to get a nonzero result, H_j must be that piece of the Hamiltonian which connects the spatial sites $(i, i+1)$ in propagating from l to $l+1$.

We can make this a little more concrete by noting the matrix element,

$$\langle\, S^z_{i,l}\, S^z_{i+1,l}|(S^+_i S^-_{i+1} + S^-_i S^+_{i+1})e^{-\tau \hat{H}_j}|\, S^z_{i,l+1}\, S^z_{i+1,l+1}\rangle, \quad (37)$$

vanishes if $S^z_{i,l} + S^z_{i+1,l} = 0, 2$. (Recall local conservation laws require that $S^z_{i,l+1} + S^z_{i+1,l+1} = S^z_{i,l} + S^z_{i+1,l}$. In this case we have either no world–lines propagating up the shaded square, or else two world–lines propagating up the square. No spin–flips are possible, and it is natural that the expectation value vanish. If, on the other hand, the plaquette has $S^z_{i,l} + S^z_{i+1,l} = 1$, then there is a non–zero contribution. The ratio of expectation values is $\tanh(J_x\Delta\tau/2)$ if the plaquette's single world–line is propagating vertically upward, and $\coth(J_x\Delta\tau/2)$ if the single world–line traverses the plaquette diagonal. That the kinetic energy is large in the latter case is intuitively appealling when the model being simulates is a fermion or boson Hamiltonian:

a world–line moving across the plaquette in which the particle is changing sites makes a large contribution the expectation value of the kinetic energy, while a world–line moving upwards does not.

Measuring an operator which does not conserve particle number locally, is even more complicated, since the resulting ratio is ill–defined. More precisely, an operator like $S_i^+ S_{i+j}^- + S_i^- S_{i+j}^+$ where $j > 1$ will result in a sequence of states in the numerator which is completely different from that in the denominator. As has been described,[1] it is possible to solve this problem by conducting two parallel simulations, one with "broken" world–lines, but in practice the technique is quite complicated, and also results in measurements which are very noisy. Most world–line simulations measure only operators which do not break world–lines. These issues are closely related to the discussion of "forward–" and "side–" walking discussed in the contributions of Nightingale and Umrigar in this volume.

We comment that it is sometimes possible to measure different sets of correlation functions by inserting different types of intermediate states in the simulation. To measure an operator like $S_i^+ S_{i+j}^- + S_i^- S_{i+j}^+ = 2(S_i^x S_{i+j}^x + S_i^y S_{i+j}^y)$, which is not diagonal in the basis of $S_{\mathbf{i}}^z$, for example, one could insert instead as intermediate states complete sets of eigenstates of S_i^x in the path–integral. Whether or not this is possible depends on the sign problem. Because the XXZ Hamiltonian does not commute with $S_{\rm tot}^x$, the eigenstates $|S_1^x = +, S_2^x = +\rangle$ and $|S_1^x = -, S_2^x = -\rangle$ are mixed, in addition to a mixing of $|S_1^x = +, S_2^x = -\rangle$ and $|S_1^x = -, S_2^x = +\rangle$. A straightforward calculation shows that there is no sign problem if one is in the Heisenberg or Ising limits $J_z \geq J_x$.

In spite of the restrictions on the operators we can measure, we shall see when we discuss lattice bosons that we are still able to extract a lot of interesting physics from world–line simulations. Because spin–1/2 systems are identical to hard–core bosons, we will defer presenting typical results from these simulations to the next section.

We have one final caveat to make about the world–line algorithm. The moves described above in which world–lines are locally deformed are not ergodic. For example, they never change the total magnetization. This is so because whole world lines are never created or destroyed, only changed in shape. There is also another, more subtle, quantity that these moves conserve: the winding number. Periodic boundary conditions require that the world lines connect across the last and first time slices in a continuous fashion. They can do this is a trivial way, with each world–line moving generally upward through the lattice (see Fig. 9a), but they can also satisfy the periodic boundary conditions in imaginary time with configurations in which there is a net flow of world–lines across the right or left spatial sides of the system (see Fig. 9b). Such configurations are said to have non–zero

winding number. Moves which are local deformations of the lattice cannot change the winding number, that is, they can never evolve from 9a to 9b.

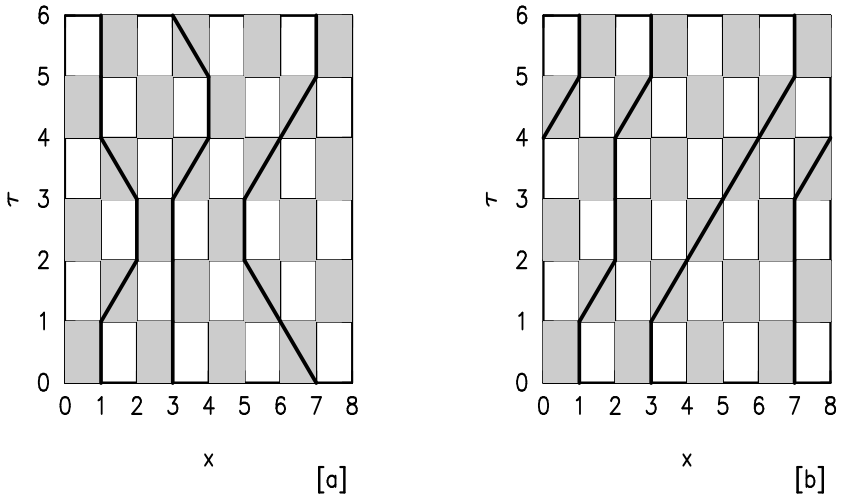

Figure 9. World–line configurations with winding number $W = 0$ [a] and $W = 1$ [b]. Both satisfy all the local conservation laws, as well as periodicity in imaginary time. No sequence of local distortions of the world–lines can evolve the system from [a] to [b].

As with the equivalence of the fixed and fluctuating particle number ensembles, in the thermodynamic limit it can be argued that the fixed winding number sector yields the same physics as allowing the winding number to fluctuate. Perhaps the simplest way to see this is that if there were no spatial periodic boundary conditions in the kinetic energy term, then winding around the lattice would not be possible. But we certainly expect that periodic and open boundary cinditions to give the same result in the thermodynamic limit. Therefore we expect the inclusion of non–zero winding moves to be unnecessary in the thermodynamic limit. It has also been been verified by explicit calculation with and without moves which change the winding number that expectation values of observables are the same in the thermodynamic limit.[18] We will come back in the next section to a discussion of these global conservation laws.

Nevertheless, the existence of these global conservation laws is a bit disconcerting. For one thing, the most natural analytic check, $J_z = 0$ (a noninteracting system in boson language) is no longer simple since the exact result includes all winding number sectors. This is especially unfortunate since the coding of the kinetic energy terms which this verifies is the most

difficult part of the world–line algorithm, and hence the most important part to check carefully. An ancillary benefit of the loop algorithms, whose primary virtue is the rapid exploration of phase space, is that they also allow for moves connecting the different magnetization and winding number sectors.

5. World–Lines for Interacting Bosons

In this section we will discuss world–line monte carlo for interacting bosons. Such simulations were first carried out[19] for continuum models of the superfluid transition in He^4, and have been more recently applied lattice models in studies of the superconductor–insulator transition in thin films.[20, 21, 22, 23, 25, 24, 26, 27, 28, 29] We first point out that the problem of hard–core bosons is isomorphic to the quantum spin–1/2 XXZ Hamiltonian considered in the previous section. We then discuss the soft–core case, and also some of the physics of interacting bosons and how it might best be extracted from QMC.

By making the identifications,

$$S_{\mathbf{i}}^{+} \rightarrow a_{\mathbf{i}}^{\dagger} \qquad S_{\mathbf{i}}^{-} \rightarrow a_{\mathbf{i}} \qquad S_{\mathbf{i}}^{z} + \frac{1}{2} \rightarrow a_{\mathbf{i}}^{\dagger} a_{\mathbf{i}} = n_{\mathbf{i}}, \tag{38}$$

we can map quantum spin–1/2 operators onto hard–core bosons. Here $a_{\mathbf{i}}(a_{\mathbf{i}}^{\dagger})$ are boson annihilation(creation) operators at site i. The hard–core constraint $n_{\mathbf{i}} = \pm 1$ guarantees that the Hilbert space has the same dimensionality, two states per site, as a spin–1/2 system. More formally, the commutation relations of the boson operators, together with Eq. 38, reproduce the appropriate spin commutation relations.

With this mapping the quantum spin Hamiltonian becomes,

$$H = -t \sum_{\langle \mathbf{ij} \rangle} (a_i^{\dagger} a_j + a_j^{\dagger} a_i) - \mu \sum_{\mathbf{i}} n_i + U_{\mathrm{hc}} + V \sum_{\langle \mathbf{ij} \rangle} n_i n_j. \tag{39}$$

In boson language, μ is the chemical potential. t is the hopping parameter, U_{hc} is a hard–core potential, and V is a near–neighbor repulsion. These quantities are related to the parameters in the spin Hamiltonian via,

$$J_{xy} \rightarrow 2t \qquad J_z \rightarrow V \qquad B \rightarrow \mu. \tag{40}$$

As we have discussed, for $J_z > J_x$ the spin Hamiltonian is in the Ising universality class, and has dominant $\langle S_{\mathbf{i}}^z S_{\mathbf{i+l}}^z \rangle$ correlations. In boson language this corresponds to a model where the interactions dominate the kinetic energy $V > 2t$ resulting in a phase where density correlations $\langle n_{\mathbf{i}} n_{\mathbf{i+l}} \rangle$ have a well defined oscillatory pattern. Meanwhile, in the opposite limit

$J_x > J_z$ the spin Hamiltonian is in the XY universality class, and has dominant $\langle S^+_{\mathbf{i}} S^-_{\mathbf{i+l}} \rangle$ correlations. In boson language this corresponds to a model where the kinetic energy dominates the interactions $2t > V$, resulting in a superfluid phase wil large off–diagonal correlations $\langle a^\dagger_{\mathbf{i}} a_{\mathbf{i+l}} \rangle$. The isotropic Heisenberg point of the spin model $J_x = J_z$ corresponds to a "supersolid" phase where the bosons have simultaneous diagonal and off–diagonal long range order.[30]

Since the two models are completely isomorphic, the discussion of the simulation method for quantum spins carries over unchanged to the hard–core boson model, apart from a trivial change in language. Note that the choice of $-t$ in front of the kinetic energy term (as opposed to $+t$), a convention which not affect the physics, prevents a sign problem. This is the same argument as we made previously for the difference in sign of J_x in the quantum spin model.

However, it is also of interest to study a soft–core "boson–Hubbard" Hamiltonian in which the hard–core constraint which forbids double occupancy is replaced by a finite repulsion $U_{\rm hc} \to U n_{\mathbf{i}}(n_{\mathbf{i}} - 1)$. It is necessary to evaluate a more general class of matrix elements,

$$\langle\, n_{\mathbf{i},l}\ n_{\mathbf{j},l} | e^{t\Delta\tau(a^\dagger_{\mathbf{i}} a_{\mathbf{j}} + a^\dagger_{\mathbf{j}} a_{\mathbf{i}})} |\, n_{\mathbf{i},l+1}\ n_{\mathbf{j},l+1} \rangle \tag{41}$$

Local particle number requires that $n_{\mathbf{i},l} + n_{\mathbf{j},l} = n_{\mathbf{i},l+1} + n_{\mathbf{j},l+1}$, but we no longer have the restriction $n_{\mathbf{i},l} = 0, 1$. The calculation of the matrix elements can be done either by diagonalizing H in a truncated Hilbert space, allowing, for example, up to a maximum of $n_{\mathbf{i}} = 10$ bosons per site,[31] or exactly.[32]

We can check a code for the generalized soft–core model against diagonalization results on a 4 site lattice. In Fig. 10 we show a comparison between the quantum simulation and the exact values for the occupations, f_m which measure the fraction of sites having m bosons. Here we have chosen $\beta = 1, L = 8, N_b = 4$ and $t = 1$, and show f_m versus U. For U large and negative, all the bosons clump on a single site, so that there is one site with four bosons and three empty ones. Thus $f_0 = \frac{3}{4}, f_1 = 0, f_2 = 0, f_3 = 0$, and $f_4 = \frac{1}{4}$. When U becomes large and positive, the bosons distribute themselves one to a site, and all f_m vanish except for f_1 which approaches one. Note again that the exact diagonalization includes all winding number sectors, yet is in good agreement with the simulations, which do not.

We now briefly describe the physics of the boson–Hubbard model in order to motivate a further discussion of the issue of particle and winding number conservation.[20, 33] Let us consider the ground state phase diagram. In the absence of any boson kinetic energy, $t = 0$, all the sites are independent and will contain a number of particles determined by the

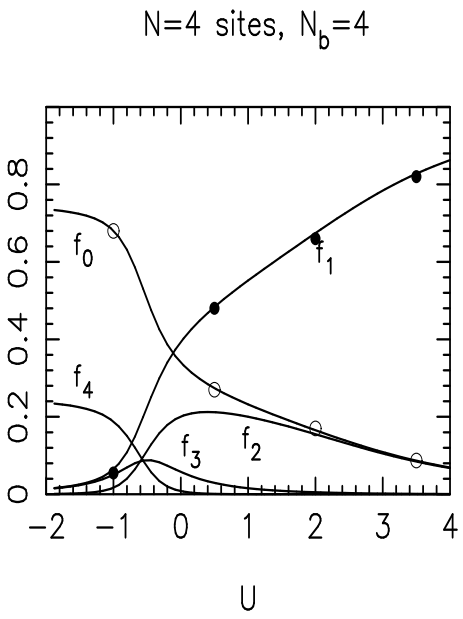

Figure 10. The fractional occupations, defined in the text, as a function of on–site repulsion U. The open(closed) circles are QMC results for $f_0(f_1)$ from a boson–Hubbard world–line code, and the smooth curves are from exact diagonalization. The lattice is four sites, as is the number of bosons.

chemical potential. If $\mu < 0$ the number of bosons on each site N_b will be zero. For chemical potentials $2(N_b-1)U < \mu < 2N_bU$, the number of bosons on each site will be N_b. A plot of the density per site $\langle n \rangle$ as a function of chemical potential μ will exhibit a set of steps when μ is an integral multiple of $2U$. The size of these steps measures the gap to charge excitations, and on these steps the compressibility $\kappa = \partial \langle n \rangle / \partial \mu = 0$, vanishes. When the hopping t is turned on, the bosons can condense into a superfluid phase, and indeed they do so immediately for incommensurate fillings. However, the plateaus where the density $\langle n \rangle$ is an integer will not be destroyed until t/U reaches a critical value. When $t/U > (t/U)_c$ the bosons will also have a superfluid ground state at commensurate filling. The qualitative phase diagram therefore consists of insulating "Mott lobes" at low t/U where the density is fixed at integer values and there is a nonzero gap Δ, and a superfluid phase outside these lobes.

Because it has insulating and superfluid phases, and a transition between them, the boson–Hubbard Hamiltonian has been used to model the superconducting–insulating phase transition in thin, disordered films, and, in particular, the issue of a possible universal conductance value at the critical point.[22, 23, 33, 34] In order to include randomness, a key ingredient

in the physics of these systems, the chemical potential in Eq. 39 is modified to depend on the site index $\mu \to \mu_{\mathbf{i}}$. This randomness competes with the interactions which drive the Mott insulating phase, since the energy cost to move an electron in a phase where all sites are singly occupied is reduced from U to $U - \epsilon$ where ϵ is the scale of the randomness. On the other hand, it is not clear that this weakening of the gap will aid the superfluid phase, since disorder generally acts against extended states as well. Indeed, it is believed that the random site energies drive the formation of a third, "Bose glass," phase in which both the gap and superfluid density vanish.[33]

It is clear from the above discussion that computation of the compressibility and superfluid density are essential to a description of the physics of the boson–Hubbard model. (In fact, some of these same issues could already have been raised in the preceding section in the context of computing the magnetic susceptibility and spin stiffness in quantum spin Hamiltonians.) How are these quantities to be measured, given the restricted ensembles in which world–line simulations are often formulated?

It is simple to make contact between fixed and variable particle number ensembles.[20] At zero temperature, the chemical potential can be expressed as the derivative of the ground state energy with respect to particle number. Replacing the derivative by a discrete difference, we have,

$$\mu(N_b) = E_0(N_b + 1) - E_0(N_b). \tag{42}$$

We can then obtain the compressibility κ,

$$\kappa(\mu) = \frac{1}{\mu(N_b + 1) - \mu(N_b)}. \tag{43}$$

Even on modest sized lattices it is possible to get an accurate determination of the phase diagram and also to evaluate the critical exponent predicted for the behavior of κ as the Mott lobe is approached by changing the chemical potential.[33, 9] Typical traces of the density $\langle n \rangle$ as a function of chemical potential are shown in Fig. 11, and the resulting phase diagram determined thereby[35] is given in Fig. 12.

The second quantity we need to measure is the order parameter for the superfluid transition. The first choice might be to evaluate the asymptotic behavior of the equal time boson Greens function $\langle a_{\mathbf{j}} a_{\mathbf{i}}^\dagger \rangle$ as $|\mathbf{i} - \mathbf{j}| \to \infty$, which is nothing more than the superfluid condensate, the macroscopic occupation of the $\mathbf{k} = 0$ mode. As we have discussed, however, this quantity cannot be measured in a world–line simulation.[36] Instead we will measure the superfluid density ρ_s, a quantity which gives the response of the energy to a twist in the boundary conditions.[36] Specifically, if the energy of a lattice of linear dimension L is measured with periodic and antiperiodic

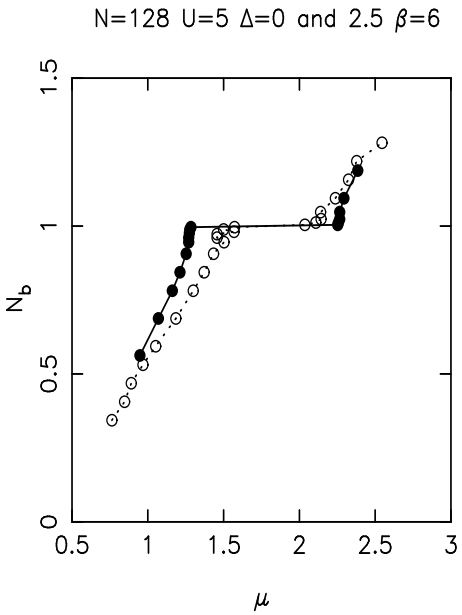

Figure 11. The occupation per site, N_b, as a function of chemical potential for fixed on–site repulsion $U = 5$ and two different disorder stengths, $\Delta = 0$ (closed circles) and $\Delta = 2.5$ (open circles). The plateau at $N_b = 1$ indicates a Mott insulating phase, and its extent measures the size of the gap. The lattice is $N = 128$ sites, and the inverse temperature $\beta = 6$.

boundary conditions, then $\rho_s = 2L(E_{\rm apbc} - E_{\rm pbc})$. Ceperley and Pollock have shown[19] that the superfluid density is proportional to the winding number $\rho_s \propto \langle W^2 \rangle$.

Unfortunately, this does not completely solve the difficulty of finding an order parameter for the superfluid phase, since our simulations are conducted in the $W = 0$ ensemble, and hence $\rho_s = 0$. However, this difficulty can be solved by considering a generalization of the winding number.[31] We define a "pseudocurrent"[37] operator $\tilde{j}(\tau)$ which measures the surplus of right moving to left moving bosons at imaginary time τ, and an associated correlation function $\mathcal{J}$.

$$\begin{aligned} \tilde{\mathcal{J}}(\tau) &= \langle \tilde{j}(\tau)\tilde{j}(0)\rangle, \\ \tilde{j}(\tau) &= \sum_{i=1}^{N_b} [x(i,\tau+1) - x(i,\tau)]. \end{aligned} \tag{44}$$

Here $x(i,\tau)$ is the position of boson i at time slice τ. The Fourier transform,

$$\mathcal{J}(\omega) = \sum_{\tau} e^{i\omega\tau} \mathcal{J}(\tau), \tag{45}$$

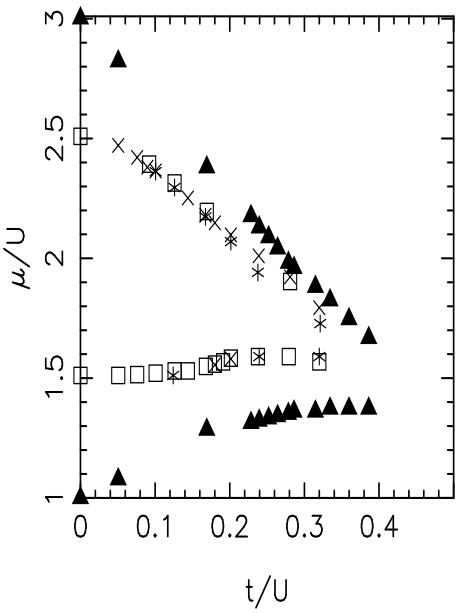

Figure 12. The boundary of the Mott insulating lobe as determined from a family of curves of $n(\mu)$ for different U as in Fig. 11. The solid triangles are for the clean system. The other symbols are for a ratio of disorder to interaction strength of 1/2, with the number of sites $N = 64$ (crosses), $N = 128$ (squares), and $N = 256$ (stars).

obeys $\tilde{\mathcal{J}}(\omega = 0) \propto \langle W^2 \rangle$, for simulations which sample all winding number sectors. In simulations constrained to $W = 0$, $\tilde{\mathcal{J}}(\omega \to 0) \propto \langle W^2 \rangle$. This procedure is analogous to measuring the magnetic susceptibility in an Ising model simulation with conserved magnetization order parameter $M = 0$ by defining a momentum dependent susceptibility and extrapolating to zero momentum.[31]

The results of such a procedure are illustrated in Fig. 13 where we show the frequency dependent pseudocurrent–pseudocurrent correlation function $\tilde{\mathcal{J}}(\omega)$ as a function of frequency ω for different values of the density. There is a very clear difference between the behavior at a density of one boson per site, where $\tilde{\mathcal{J}}(\omega \to 0) = 0$ and away from that density, where $\tilde{\mathcal{J}}(\omega \to 0)$ does not vanish. This tells us that the gapped Mott phase has $\rho_s = 0$ while the region away from density one where $\kappa is finite$ is a superfluid. At weaker coupling, $t/U > (t/U)_c$, we find that ρ_s becomes nonzero even at commensurate filling, just at the same point where the gap vanishes. However, in the disordered system there is a phase where the gap vanishes but ρ_s is still zero. This is the "Bose glass".

We conclude this section by noting that the first simulations of superfluid transitions for interacting bosons were calculated for continuum

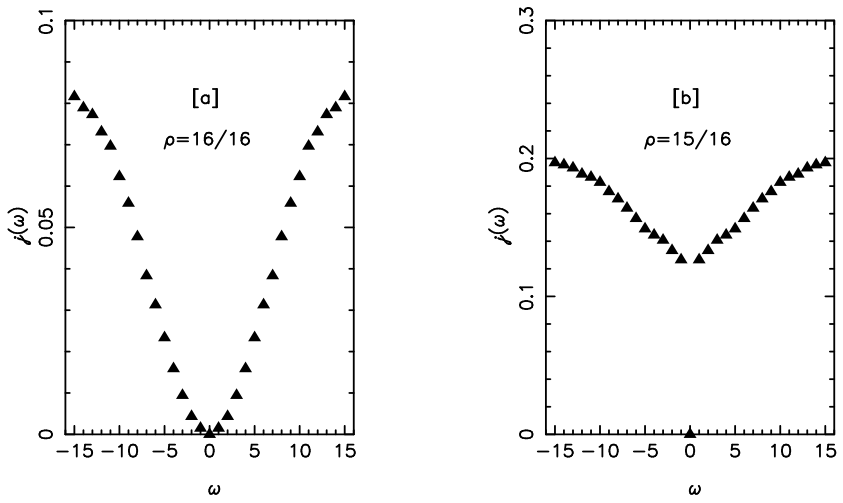

Figure 13. The pseudocurrent–pseudocurrent correlation function versus frequency (circles). Panel (a) shows 16 bosons on 16 sites, and panel (b) shows 15 bosons on 16 sites. In the latter case, the extrapolation $\omega \to 0$ yields a non–zero value, different from the $\omega = 0$ value which is pinned to zero by the constraint $W = 0$. This is therefore a superfluid. In both cases, the inverse temperature $\beta = 2$ and the on–site repulsion $U = 20$.

models.[19] Beginning with a first quantized Hamiltonian,

$$H = \sum_i \frac{\vec{P}_i^2}{2m} + \sum_{i,j} V(\vec{X}_i - \vec{X}_j), \tag{46}$$

the inverse temperature is discretized and complete sets of continuous position eigenstates are inserted between the operators $e^{-\Delta\tau H_n}$. Just as in our discussion of the quantum oscillator, the expression which results consists of a classical problem of a set of interacting chains $\vec{x}_i(\tau)$ which represent the trajectory of each boson in imaginary time. However, in addition to moves which modify the boson positions, it is also essential to include moves which guarantee that the boson wavefunction is symmetric. This turns out to require "exchange" moves which connect the chains corresponding to different bosons.

The resulting simulations give an appealing qualitative picture of the nature of the superfluid transition.[19] At high temperatures, the individual chains do not have much "imaginary time" to wander, so that if one projects the coordinates $\vec{x}_i(\tau)$ down to the $\tau = 0$ plane they form fairly small closed trajectories. Their size is roughly given by the deBroglie ther-

mal wavelength $\lambda_{\rm T} = h/\sqrt{2\pi m k_B T}$. As the temperature is lowered, the chains have an increasing length of imaginary time in which to wander, and the projected path becomes larger and larger. Eventually, the paths of different bosons begin to become close enough for the exchange moves to be accepted, signaling the superfluid transition. The exchange moves also allow the winding number to change, so that $\langle W^2 \rangle$ can be directly measured to probe the superfluid transition quantitatively. A technical difficulty is that the acceptance rate of the exchange moves falls as the system size is increased, providing a limit to the size of the systems that can be easily simulated.[19]

6. World–Lines for Interacting Fermions

Our final illustration of the world–line algorithm is for lattice fermions. Because both the physics and the algorithm have been described several times,[1] we present only a short discussion which sets forth some of the differences with the boson case. Consider first, for concreteness, a model of one–dimensional spinless fermions with a repulsion V between near–neighbor sites.

$$H = -t \sum_i (c_i^\dagger c_{i+1} + c_{i+1}^\dagger c_i) - \mu \sum_i n_i + V \sum_i n_i n_{i+1}. \tag{47}$$

As with lattice bosons, the formulation of the algorithm resembles that of a quantum spin–1/2 Hamiltonian very closely. The Pauli principle automatically enforces a "hard–core" constraint which forbids us from considering the generalization to multiple occupancy. The only non–zero matrix elements are, abbreviating $\hat{h}_i = -t\Delta\tau(c_i^\dagger c_{i+1} + c_{i+1}^\dagger c_i)$,

$$\begin{aligned}
\langle\, 0\,0 \,|e^{-\hat{h}_i}|\, 0\,0 \,\rangle &= 1, \\
\langle\, 1\,0 \,|e^{-\hat{h}_i}|\, 1\,0 \,\rangle = \cosh(t\Delta\tau), &\qquad \langle\, 1\,0 \,|e^{-\hat{h}_i}|\, 0\,1 \,\rangle = \sinh(t\Delta\tau), \\
\langle\, 0\,1 \,|e^{-\hat{h}_i}|\, 1\,0 \,\rangle = \sinh(t\Delta\tau), &\qquad \langle\, 0\,1 \,|e^{-\hat{h}_i}|\, 0\,1 \,\rangle = \cosh(t\Delta\tau), \\
\langle\, 1\,1 \,|e^{-\hat{h}_i}|\, 1\,1 \,\rangle &= 1.
\end{aligned} \tag{48}$$

These matrix elements are identical to those arising in the spin–1/2 XXZ model, Eq. 34, and the hard–core boson model. This similarity in the world–line algorithm for the different models reflects, of course, the exact mappings which exist between all these systems in one dimension.

For more general fermion Hamiltonians, world–line algorithms differ from those for quantum spins and bosons in two ways. First, in the fermion case, one is typically interested in models in which the operators also carry a spin index. (Of course there are instances of quantum spin and boson

models where there are several spin or boson species, but such cases are the exception, whereas for fermions they are the rule.) When there are only density–density interactions of the form $n_{i\uparrow}n_{j\downarrow}$ coupling the two spin species, that is, no spin flip hopping terms like $c^\dagger_{i\uparrow}c_{j\downarrow}$ or more complicated interactions like $c^\dagger_{i\uparrow}c_{i\downarrow}c^\dagger_{j\downarrow}c_{j\uparrow}$, then the path–integral which arises involves two *separate* checkerboard lattices. That is, the off–diagonal matrix elements involve only one spin species at a time, and the coupling between the spin species is through the diagonal terms which factor out of the matrix elements as numbers. Thus one suggests moves which distort fermion world–lines of one spin species leaving the other spin species' world–lines unchanged, though this static configuration of the other spin species does enter the acceptance–rejection decision through the diagonal interaction terms.

The second, and much more profound, difference is in the sign problem. Boson and quantum spin operators have non–zero commutation relations on the same site, but *commute* on different sites. This means that the sign of the matrix elements entering the simulation is determined completely locally, for example by the explicit solution of the two site problem which arises after the checkerboard decomposition. Fermion operators, on the other hand, *anticommute* on different sites. Additional minus signs can arise in getting the fermion creation operators in their canonical order after a hopping process.

To be more specific, recall that in expressing a fermion occupation number state like $|1\,0\,1\,1\,0\ldots\rangle$ a convention for the order in which the creation operators act on the vacuum must be chosen. For example we might define $|1\,1\,0\,1\,0\ldots\rangle = c^\dagger_1 c^\dagger_2 c^\dagger_4 \ldots |\mathrm{vac}\rangle$. Consider the action of $c^\dagger_3 c_4$ on this state. We anticommute the *pair* of operators through $c^\dagger_1$ and $c^\dagger_2$, but since we are moving two operators together there are no sign changes. At this point, the destruction operator for site 4 meets the creation operator on site 4 and they cancel. The crucial point to observe is that this whole process leaves the creation operators in their canonical order $c^\dagger_1 c^\dagger_2 c^\dagger_3 \ldots |\mathrm{vac}\rangle$ so we get the occupation number state $|1\,1\,1\,0\,0\ldots\rangle$ with no minus sign.

What would happen if we instead acted with a longer range hopping $c^\dagger_5 c_2$ on this state? This pair of operators would anticommute through $c^\dagger_1$ without introducing a minus sign. $c^\dagger_2$ would then meet and destroy c_2, but $c^\dagger_5$ would be left out of its canonical order, that is, to the left of $c^\dagger_4$. Anticommuting it through yields $-|1\,0\,0\,1\,1\ldots\rangle$. This minus sign introduces large fluctuations into measurements and prevents useful simulations. The general rule is that one gets a minus sign if there is an odd number of occupied sites "in between" the two states that are connected by the hopping, where "in between" means the order of creation operators in the convention chosen for

acting on the vacuum state. One does not need to have long–range hopping to encounter this problem. If one has a two–dimensional lattice and has a convention for occupation number states in which the operators for rows in the x direction are adjacent, the hopping in the y direction will be between sites which are not "neighbors" in the string of creation operators. Such hopping processes will yield minus signs.

Fermion world–line simulations are not possible except strictly in one dimension. Even a one–dimensional lattice with a single "impurity" orbital onto which the fermions can hop will have a sign problem. As we have discussed, hoppings which are longer range than near–neighbor cannot be handled. An exception is the case when only interactions, and not kinetic energy terms couple one–dimensional chains along which the fermions hop. Thus the world–line algorithm for fermions is almost exclusively applied to models in one–dimension. Many path integral QMC simulations of interacting fermions in higher dimension are conducted with the determinant algorithm described in this volume.

We conclude by mentioning that nice illustrations of the real space spin density wave, charge density wave, and other correlations in fermion models treated by the world–line method can be found in Ref. [1].

7. Finite Size Scaling in Quantum Phase Transitions

Finite size effects are the most important limitation of monte carlo simulations. In this section we present a brief discussion of an additional feature of finite size scaling (FSS) in quantum simulations.

We begin by reviewing some of the elements of FSS for a classical system like the Ising model which exhibits a second order phase transition. In an infinite system, near a second order critical point, quantities like the specific heat, magnetization, susceptibility, and correlation length exhibit power law singularities,

$$C \propto t^{-\alpha} \qquad M \propto t^{-\beta} \qquad \chi \propto t^{-\gamma} \qquad \xi \propto t^{-\nu}. \tag{49}$$

Here $t = |T - T_c|$ is the distance from the critical point and $\alpha, \beta, \gamma, \nu$ are critical exponents whose values we are interested in calculating.

For a finite system, these quantities will of course depend on the linear system size N in addition to t. The fundamental assumption of FSS is that the functional dependence on N and t is such that only the ratio $N/\xi = Nt^{\nu}$ enters. Thus for the susceptibility we write,

$$\chi(N, t) \propto N^{\frac{\gamma}{\nu}} f(Nt^{\nu}), \tag{50}$$

where f is some unspecified FSS function. This form embodies the dependence on the ratio of correlation length to system size, and also reduces to

the correct form $\chi \propto t^{-\gamma}$ when $N \to \infty$. Thus a simple version of FSS for classical second order phase transitions is to plot the scaled susceptibility $N^{-\frac{\gamma}{\nu}}\chi(N,t)$ versus the scaling variable Nt^{ν}. Data for different lattice sizes should all lie on a single "universal curve," allowing for a determination of the exponents γ and ν, and the critical temperature T_c, based on the quality of this data collapse.

In the case of quantum systems we are often interested in "quantum" phase transitions which occur in the ground state as a function of some control parameter other than the temperature. For example, as we discussed in section 3, the ground state of the Ising model in a transverse field undergoes a phase transition at $T = 0$. Similarly the boson–Hubbard model undergoes an insulator–superfluid transition at $T = 0$ as the hopping is increased. Just as we cannot simulate spatial size $N = \infty$, we are also restricted to finite L instead of $\beta = infty$. Thus, in such quantum mechanical problems the quantities measured will depend not only on the spatial size N but also on the imaginary time size L. FSS can still be done, but it is necessary also to keep the aspect ratio of the system, N^z/L fixed as the spatial size N is varied. Here z is the dynamical critical exponent. Physically, this reflects the statement that the correlation length in imaginary time diverges as $\xi_\tau \propto \xi^z$. The ratio ξ^z/ξ_τ also enters the scaling function and in order to get collapse of data for different system sizes, this quantity must be kept fixed in the simulation. This is a more serious problem than just giving another fitting parameter in addition to the other exponents and the position of the critical point, since z controls the aspect ratio of the lattices to be simulated.

8. Conclusions

The world–line QMC algorithm is a powerful approach to the simulation of lattice quantum spin, boson, and fermion models. It is considerably more pictorial than other QMC methods like the determinant algorithm. It also has a local action which results in a nominally linear scaling with system size for a sweep through the lattice updating all the degrees of freedom.

However, the technique also has a number of drawbacks: The difficulty in measuring certain observables, the sign problem which prevents the study of frustated spin models or fermions in greater than one dimension, and long equilibration and autocorrelation times. A number of these difficulties have been solved by the construction of loop algorithms.[3]

Acknowledgements

This work was supported by the (US) National Science Foundation through Grant DMR-9816170.

References

1. J.E. Hirsch, R.L. Sugar, D.J. Scalapino and R. Blankenbecler, Phys. Rev. **B26**, 5033 (1982).
2. R. Blankenbecler, R.L. Sugar, and D.J. Scalapino, Phys. Rev. **D24**, 2278 (1981).
3. R.H. Swendsen and J.–S. Wang, Phys. Rev. Lett. **58**, 86 (1987). N. Kawashima, J.E. Gubernatis, and H.G. Evertz, Phys. Rev. **B50**, 136 (1994); N.V. Prokofev, B.V. Svistunov, and I.S. Tupitsyn, JETP Lett. **64**, 911 (1996); and B.B. Beard, and U.–J. Wiese, Phys. Rev. Lett. **77**, 5130 (1997).
4. This discussion of the path integral for the partition function for the quantum oscillator is, of course, almost identical to Feynman's original formulation for the real time evolution operator $e^{-i\hat{H}t}$. See R.P. Feynman and A.R. Hibbs, *Quantum Mechanics and Path Integrals*, McGraw–Hill, 1965.
5. An extensive discussion of path integral monte carlo approaches to solve the quantum harmonic oscillator problem can be found in the seminal article by M. Creutz and J. Freedman, Annals of Phys. **132**, 427 (1981).
6. H.F. Trotter, Proc. Am. Math. Soc. **10**, 545 (1959); and M. Suzuki, Phys. Lett. **113A**, 299 (1985).
7. R.M. Fye, Phys. Rev. **B33**, 6271 (1986).
8. One can also employ "higher-order" Trotter approximations,

   $$e^{-\Delta\tau(\hat{H}_1+\hat{H}_2)} \approx e^{-\frac{1}{2}\Delta\tau\hat{H}_1}e^{-\Delta\tau\hat{H}_2}e^{-\frac{1}{2}\Delta\tau\hat{H}_1},$$

   whose error is order $(\Delta\tau)^3$. However, when this expression is put inside the trace to calculate the partition function Z, it is identical to the approximation

   $$e^{-\Delta\tau(\hat{H}_1+\hat{H}_2)} \approx e^{-\Delta\tau\hat{H}_1}e^{-\Delta\tau\hat{H}_2}.$$

   A considerable literature exists on different schemes for breaking up the exponential of H. In the "Greens Function Monte Carlo" community, the question of the Trotter approximation is often referred to as the problem of choosing a good "high temperature propagator," since after the division of β each exponential now describes a problem at a temperature higher by the factor L.
9. R. Gupta, J. DeLapp, G. Batrouni, G. Fox, C. Baillie, and J. Apostolakis, Phys. Rev. Lett. **61** 1996 (1988). See also the contribution by David Freeman in this volume.
10. D.S. Fisher, Phys. Rev. **B51**, 6411 (1995).
11. A.P. Young and H. Rieger, Phys. Rev. **B53**, 8486 (1996).
12. K. Binder, *Monte Carlo Methods in Statistical Physics*, K. Binder (ed), Springer, New York (1986).
13. The most efficient way of treating the one–dimensional model is not with QMC but rather by using the Jordan–Wigner transformation to map the model onto a non–interacting, disordered fermion problem which can be solved with exact diagonalization. See Ref. 11.
14. J.D. Reger and A.P. Young, Phys. Rev. **B37**, 5978 (1988).
15. M. Barma and B.S. Shastry, Phys. Rev. **B18**, 3351 (1978).
16. E. Loh, Jr., D.J. Scalapino, and P.M. Grant, Phys. Rev. **B31**, 4712 (1985).
17. Techniques required to stabilize the determinant algorithm can introduce additional operations which scale as higher powers of L. See G. Sugiyama and S.E. Koonin, *Ann. Phys.* **168**, 1 (1986); S. Sorella, E. Tosatti, S. Baroni, R. Car, and M. Parrinello, *Int. J. Mod. Phys.* **B1**, 993 (1989); and S.R. White, D.J. Scalapino, R.L. Sugar, E.Y. Loh, Jr., J.E. Gubernatis, and R.T. Scalettar, Phys. Rev. **B40**, 506 (1989).
18. M.S. Makivic, Phys. Rev. **B46**, 3167 (1992).
19. E.L. Pollock and D.M. Ceperley, Phys. Rev. **B30**, 2555 (1984); D.M. Ceperley and E.L. Pollock, Phys. Rev. Lett. **56**, 351 (1986); and E.L. Pollock and D.M. Ceperley, Phys. Rev. **B36**, 8343 (1987).

20. G.G. Batrouni, R.T. Scalettar and G.T. Zimanyi, Phys. Rev. Lett. **65**, 1765 (1990); and R.T. Scalettar, G.G. Batrouni, and G.T. Zimanyi, Phys. Rev. Lett. **66**, 3144 (1991).
21. N. Trivedi, D.M. Ceperley, and W. Krauth, Phys. Rev. Lett. **67**, 2307 (1991).
22. M. Cha, M.P.A. Fisher, S.M. Girvin, M. Wallin, and A.P. Young, Phys. Rev. **B44**, 6883 (1991).
23. E.S. Sorensen, M. Wallin, S.M. Girvin, and A.P. Young, Phys. Rev. Lett. **69**, 828 (1992).
24. K.J. Runge, Phys. Rev. **B45**, 13136 (1992).
25. K. G. Singh and D. S. Rokhsar, Phys. Rev. **B46**, 3002 (1992), K. G. Singh and D. S. Rokhsar, Phys. Rev. **B49**, 9013 (1994).
26. I.F. Herbut, Phys. Rev. **B57**, 13729 (1998).
27. N.V. Prokof'ev and B.V. Svistunov, cond–mat/9706169.
28. R.V. Pai, R. Pandit, H.R. Krishnamurthy, and S. Ramashesha Phys. Rev. Lett. **76**, 2937 (1996).
29. J. Kisker and H. Rieger, Phys. Rev. **B57**, 13729 (1998).
30. G.G. Batrouni, R.T. Scalettar, G.T. Zimanyi, and A.P. Kampf, Phys. Rev. Lett., **74** 2527 (1994); and R.T. Scalettar, G.G. Batrouni, A.P. Kampf, and G.T. Zimanyi, Phys. Rev. **B51**, 8467 (1995).
31. G.G. Batrouni and R.T. Scalettar, Phys. Rev. **B46**, 9051 (1992).
32. N. Hatano, J. Phys. Soc. of Japan **64** 1529 (1995).
33. M.P.A. Fisher, P.B. Weichman, G. Grinstein, and D.S. Fisher, Phys. Rev. **B40**, 546 (1989).
34. G.G. Batrouni, B. Larson, R.T. Scalettar, J. Tobochnik, and J. Wang, Phys. Rev. **B48**, 9628.
35. Series expansion techniques have yielded remarkable agreement, and even significant improvement, over the QMC determination of the phase diagram. See J. K. Freericks and H. Monien, Europhys. Lett. **26**, 545 (1994); J. Freericks and H. Monien, Phys. Rev. **B53**, 2691 (1996).
36. Actually, there is a further subtlety. In two dimensions the superfluid phase transition is of the Kosterlitz–Thouless type, that is, between a high temperature phase where the boson Greens function $\langle a_{\mathbf{i}}^\dagger a_{\mathbf{j}} \rangle$, falls exponentially with $|\mathbf{i}-\mathbf{j}|$, and a low temperature phase where it decreases as a power law. Thus the large separation value of the Greens function is zero even in the superfluid phase, and it is preferable to use the superfluid density ρ_s as the order parameter, even apart from numerical considerations. In the language of quantum spins, the spin–spin correlations of the XY model in two dimensions decay to zero as a power law even in the low temperature phase, but the spin stiffness, a measure of the response of the energy to a twist of the boundary conditions, is nonzero.
37. We distinguish this from the *true* current operator $j(\tau) = \sum_i (a_{i+1}^\dagger(\tau) a_i(\tau) - a_i^\dagger(\tau) a_{i+1}(\tau))$ which is used to measure the conductivity.